

Geophysical Research Letters®



RESEARCH LETTER

10.1029/2023GL104762

Key Points:

- We test if the standard plasma–magnetic field relations for magnetosonic waves are altered by standing structure or inhomogeneous plasma
- The interference pattern present in standing (body or surface) waves can lead to anomalous results under certain plasma conditions
- Advection by the wave of plasma inhomogeneities can also result in reversed correlations if gradients are sufficiently large

Supporting Information:

Supporting Information may be found in the online version of this article.

Correspondence to:

M. O. Archer,
m.archer10@imperial.ac.uk

Citation:

Archer, M. O., Southwood, D. J., Hartinger, M. D., Rastätter, L., & Nykyri, K. (2023). Magnetosonic ULF waves with anomalous plasma–magnetic field correlations: Standing waves and inhomogeneous plasmas. *Geophysical Research Letters*, 50, e2023GL104762. <https://doi.org/10.1029/2023GL104762>

Received 30 MAY 2023

Accepted 11 AUG 2023

Author Contributions:

Conceptualization: M. O. Archer

Data curation: M. D. Hartinger, L. Rastätter

Formal analysis: M. O. Archer

Investigation: M. O. Archer

Methodology: M. O. Archer, D. J. Southwood

Validation: M. O. Archer, D. J. Southwood

Visualization: M. O. Archer





Writing – original draft: M. O. Archer

Writing – review & editing: D. J. Southwood, M. D. Hartinger, K. Nykyri

© 2023. The Authors.

This is an open access article under the terms of the [Creative Commons Attribution License](https://creativecommons.org/licenses/by/4.0/), which permits use, distribution and reproduction in any medium, provided the original work is properly cited.

Magnetosonic ULF Waves With Anomalous Plasma–Magnetic Field Correlations: Standing Waves and Inhomogeneous Plasmas

M. O. Archer¹ , D. J. Southwood¹ , M. D. Hartinger² , L. Rastätter³, and K. Nykyri⁴ 

¹Space and Atmospheric Physics Group, Department of Physics, Imperial College London, London, UK, ²Space Science Institute, Boulder, CO, USA, ³NASA Goddard Space Flight Center, Greenbelt, MD, USA, ⁴Embry–Riddle Aeronautical University, Daytona Beach, FL, USA

Abstract Ultra-low frequency (ULF) wave observations across the heliosphere often rely on the sign of correlations between plasma (density/pressure) and magnetic field perturbations to distinguish between fast and slow magnetosonic modes. However, the assumptions behind this magnetohydrodynamic result are not always valid, particularly within the magnetosphere which is inhomogeneous and supports standing waves along the geomagnetic field. Through theory and a global simulation, we find both effects can result in anomalous plasma–magnetic field correlations. The interference pattern in standing waves can lead both body and surface magnetosonic waves to have different cross-phases than their constituent propagating waves. Furthermore, if the scale of gradients in the background are shorter than the wavelength or the waves are near-incompressible, then advection by the wave of inhomogeneities can overcome the wave's inherent sense of compression. These effects need to be allowed for and taken into account when applying the typical diagnostic to observations.

Plain Language Summary Fluid plasma wave theory provides a key distinguishing feature between the two compressional wave modes: fast magnetosonic waves should have correlated fluctuations in the magnetic field strength and the plasma (density or pressure) whereas anticorrelation relates to the slow magnetosonic mode. This classic result is often used as a diagnostic for waves observed by spacecraft throughout the heliosphere. However, it is important to recognize that this result is derived under the assumption of a single traveling wave in a uniform background plasma. Planetary magnetospheres, in contrast, have spatially-varying plasma conditions and can reflect waves off of boundaries to form standing modes. We investigate what influence these effects have on both freely propagating waves and those tied to a surface through analytic theory and a global magnetospheric simulation. We find it is possible for the wave's correlation between plasma and magnetic field to be fundamentally altered. For standing waves we show the interference pattern present can lead to this change, whereas for non-uniform plasmas changes are due to the wave moving plasma with a significantly different background value. These effects need to be allowed for and taken into account when applying the typical plasma–magnetic field test to observed waves.

1. Introduction

Ultra-low frequency (ULF) waves, with frequencies $\lesssim 1$ Hz (Jacobs et al., 1964), provide one means of coupling disparate regions/populations of geospace such as the solar wind, magnetosphere, plasmasphere, ring current, radiation belt, and ionosphere plasmas (Hartinger et al., 2022, and references therein). They are typically approximated using Ideal-Magnetohydrodynamics (MHD), where waves are derived about equilibrium (subscript 0's in equations) by linearizing the equations for small perturbations (δ 's), arriving at the Alfvén, and fast and slow magnetosonic dispersion relations. Number density (n) and isotropic pressure (p) fluctuations in terms of displacement ξ , where velocity $\delta \mathbf{v} = \partial \xi / \partial t$, are

$$\begin{aligned} \delta n &= -n_0 \nabla \cdot \xi - \xi \cdot \nabla n_0 \\ &= -n_0 \nabla \cdot \xi_{\perp} - n_0 \nabla \cdot \xi_{\parallel} - \xi_{\perp} \cdot \nabla n_0 - \xi_{\parallel} \cdot \nabla n_0 \end{aligned} \quad (1)$$

$$\begin{aligned} \delta p &= -\gamma p_0 \nabla \cdot \xi - \xi \cdot \nabla p_0 \\ &= -\gamma p_0 \nabla \cdot \xi_{\perp} - \gamma p_0 \nabla \cdot \xi_{\parallel} - \xi_{\perp} \cdot \nabla p_0 - \xi_{\parallel} \cdot \nabla p_0 \end{aligned} \quad (2)$$

for adiabatic exponent $\gamma = 5/3$. These consist of terms relating to the wave's inherent compression as well as advection by the wave of inhomogeneities in the background. Magnetic field strength perturbations

$$\begin{aligned}\delta B_{\parallel} &= [\nabla \times (\xi \times \mathbf{B}_0)]_{\parallel} \\ &= -B_0 \nabla \cdot \xi_{\perp} - [(\xi_{\perp} \cdot \nabla) \mathbf{B}_0]_{\parallel}\end{aligned}\quad (3)$$

are subject to similar effects, though only depend on perpendicular displacements whereas plasma compressions are sensitive to the parallel direction also.

In an infinite uniform plasma, propagating fast and slow magnetosonic body modes have (angular) frequencies

$$\omega_{F,S}^2 = \frac{1}{2} (k_{\perp}^2 + k_{\parallel}^2) (c_S^2 + v_A^2) \pm \frac{1}{2} (k_{\perp}^2 + k_{\parallel}^2) \sqrt{(c_S^2 + v_A^2)^2 - 4c_S^2 v_A^2 \frac{k_{\parallel}^2}{k_{\perp}^2 + k_{\parallel}^2}}\quad (4)$$

(v_A and $c_S = \sqrt{\gamma\beta/2}v_A$ are the Alfvén and sound speeds) and associated displacements

$$\xi \propto \left[(\omega_{F,S}^2 - k_{\parallel}^2 c_S^2) \hat{\mathbf{k}}_{\perp} + k_{\perp} k_{\parallel} c_S^2 \hat{\mathbf{B}}_0 \right] \exp\{i(\mathbf{k} \cdot \mathbf{r} - \omega_{F,S} t)\}\quad (5)$$

Equations 1–5 lead to

$$\frac{\delta n}{n_0} = \frac{\delta p}{\gamma p_0} \propto -ik_{\perp} \omega_{F,S}^2 \exp\{i(\mathbf{k} \cdot \mathbf{r} - \omega_{F,S} t)\}\quad (6)$$

$$\frac{\delta B_{\parallel}}{B_0} \propto -ik_{\perp} (\omega_{F,S}^2 - k_{\parallel}^2 c_S^2) \exp\{i(\mathbf{k} \cdot \mathbf{r} - \omega_{F,S} t)\}\quad (7)$$

thus

$$\frac{\delta B_{\parallel}}{B_0} = \left(1 - \frac{k_{\parallel}^2 c_S^2}{\omega_{F,S}^2}\right) \frac{\delta n}{n_0} = \left(1 - \frac{k_{\parallel}^2 c_S^2}{\omega_{F,S}^2}\right) \frac{\delta p}{\gamma p_0}\quad (8)$$

demonstrating (via Equation 4) that fast-modes have correlated plasma (density/pressure) and magnetic field strength perturbations, whereas slow-modes exhibit anticorrelation.

In addition to body modes, magnetosonic surface waves occur on discontinuities such as the magnetopause and plasmopause (Chen & Hasegawa, 1974; Pu & Kivelson, 1983a, 1983b; Southwood, 1968). Surface wave frequency depends on conditions from both sides of the boundary. While the compressible plasma relation can only be solved numerically, in the incompressible limit ($c_S \rightarrow \infty$) it becomes

$$\begin{aligned}\omega_{Su}^2 &= k_{\parallel}^2 \frac{B_{\text{sph}}^2 + B_{\text{msh}}^2 \left(\cos\theta_B + \frac{k_{\perp}}{k_{\parallel}} \sin\theta_B \right)^2}{\mu_0(\rho_{\text{sph}} + \rho_{\text{msh}})} \\ &\approx k_{\parallel}^2 \frac{B_{\text{sph}}^2}{\mu_0 \rho_{\text{msh}}}\end{aligned}\quad (9)$$

applied to the magnetopause with magnetic shear θ_B and negligible flows (Archer & Plaschke, 2015; Plaschke & Glassmeier, 2011). Surface waves are evanescent on either side and their (imaginary) normal wavenumber is dictated by the local magnetosonic relation

$$k_n^2 = -k_t^2 + \frac{\omega^4}{v_A^2 \omega^2 + c_S^2 (\omega^2 - k_{\parallel}^2 v_A^2)}\quad (10)$$

for tangential wavenumber k_t (note $k_n^2 = -k_t^2$ in the incompressible limit). Both quasi-fast and quasi-slow surface waves are possible in compressible theory and typically follow the same plasma–magnetic field correlations as their body wave namesakes (Pu & Kivelson, 1983a, 1983b).

The relationship between plasma and magnetic field has become a widely applied diagnostic for waves measured in situ: fast-modes have been observed in the foreshock (e.g., Eastwood et al., 2002), magnetosheath (e.g., Turc

et al., 2022), and magnetosphere (e.g., Hartinger et al., 2013); and slow-modes reported in the solar wind (e.g., Yao et al., 2013), flank magnetosphere (e.g., Zhang et al., 2022), and magnetotail (e.g., Du et al., 2011). However, given magnetospheric plasmas are highly inhomogeneous (Moore et al., 1987), with curvilinear magnetic field geometries (Degeling et al., 2010), and reflecting boundaries present (Allan, 1982; Chen & Hasegawa, 1974; Kivelson & Southwood, 1988; Southwood, 1974), it is not clear whether these relations remain universally valid. In this paper we consider the effects of standing structure and inhomogeneous plasmas on this correlation in both simple theory and a global magnetospheric simulation.

2. Theory

We apply analytic MHD theory to a box model magnetosphere (e.g., Chen & Hasegawa, 1974; Radoski, 1971; Southwood, 1974) with representative dayside conditions. An infinitesimally-thin magnetopause is located at $x = 0$ such that $x > 0$ is the magnetospheric half-space and $x < 0$ the magnetosheath. The geomagnetic field is assumed uniform at 60 nT along z . Perfectly reflecting ionospheric boundaries are placed at $z = \pm 15 R_E$ where $\xi_{\perp} = 0$, a reasonable assumption for magnetosonic waves (Kivelson & Southwood, 1988). Only if conjugate ionospheres have different conductivities might results be affected due to both standing and propagating components being present (Allan, 1982), though this effect should be small due to waves' high reflectivity. To satisfy the boundary conditions, fundamental (half-wavelength along the field) eigenmodes are considered ($\pi/k_z = 30 R_E$). The background magnetosheath and magnetospheric densities at the magnetopause are $n_{\text{msh}} = n_0(x = 0^-) = 20 \text{ cm}^{-3}$ and $n_{\text{sph}} = n_0(x = 0^+) = 1 \text{ cm}^{-3}$ respectively.

2.1. Standing Waves

Here we consider whether standing (nodal) structure along the field between conjugate ionospheres (Kivelson & Southwood, 1988) alters the plasma–magnetic field correlation. Both model half-spaces are assumed uniform and we only consider stable waves. Given the ionospheric boundary conditions, standing waves take the form (see Text S1 in Supporting Information S1).

$$\xi = \begin{pmatrix} \xi_x \cos k_z z \\ \xi_y \cos k_z z \\ \xi_z \sin k_z z \end{pmatrix} \exp\{i(\mathbf{k}_{\perp} \cdot \mathbf{r} - \omega t)\} \quad (11)$$

We do not consider perpendicular standing structure, such as in cavity/waveguide modes (Kivelson et al., 1984; Kivelson & Southwood, 1985; Samson et al., 1992).

2.1.1. Body Waves

Body wave solutions can be simply constructed by superposing waves (Equation 5) with equal perpendicular but opposite field-aligned wavenumbers, yielding

$$\xi = \begin{pmatrix} 0 \\ \left[\omega_{\text{F,SI}}^2 - k_z^2 c_S^2 \right] \cos k_z z \\ k_y k_z c_S^2 \sin k_z z \end{pmatrix} \exp\{i(k_y y - \omega_{\text{F,SI}} t)\} \quad (12)$$

It follows that the plasma–magnetic field cross-phase is determined by

$$\begin{aligned} \frac{\nabla \cdot \xi}{\nabla \cdot \xi_{\perp}} &= 1 + \frac{\nabla \cdot \xi_{\parallel}}{\nabla \cdot \xi_{\perp}} \\ &= 1 - i \left(\frac{\omega_{\text{F,SI}}^2}{k_z^2 c_S^2} - 1 \right)^{-1} \end{aligned} \quad (13)$$

Figures 1a–1d shows standing fast-modes with varying β for fixed small $k_y = k_z/2$. Relative displacement coefficients (normalized to unity; panel b) go from predominantly perpendicular (purple) to parallel (blue) with increasing β . Standing waves exhibit quadrature between compression (divergence of displacement) in the parallel and

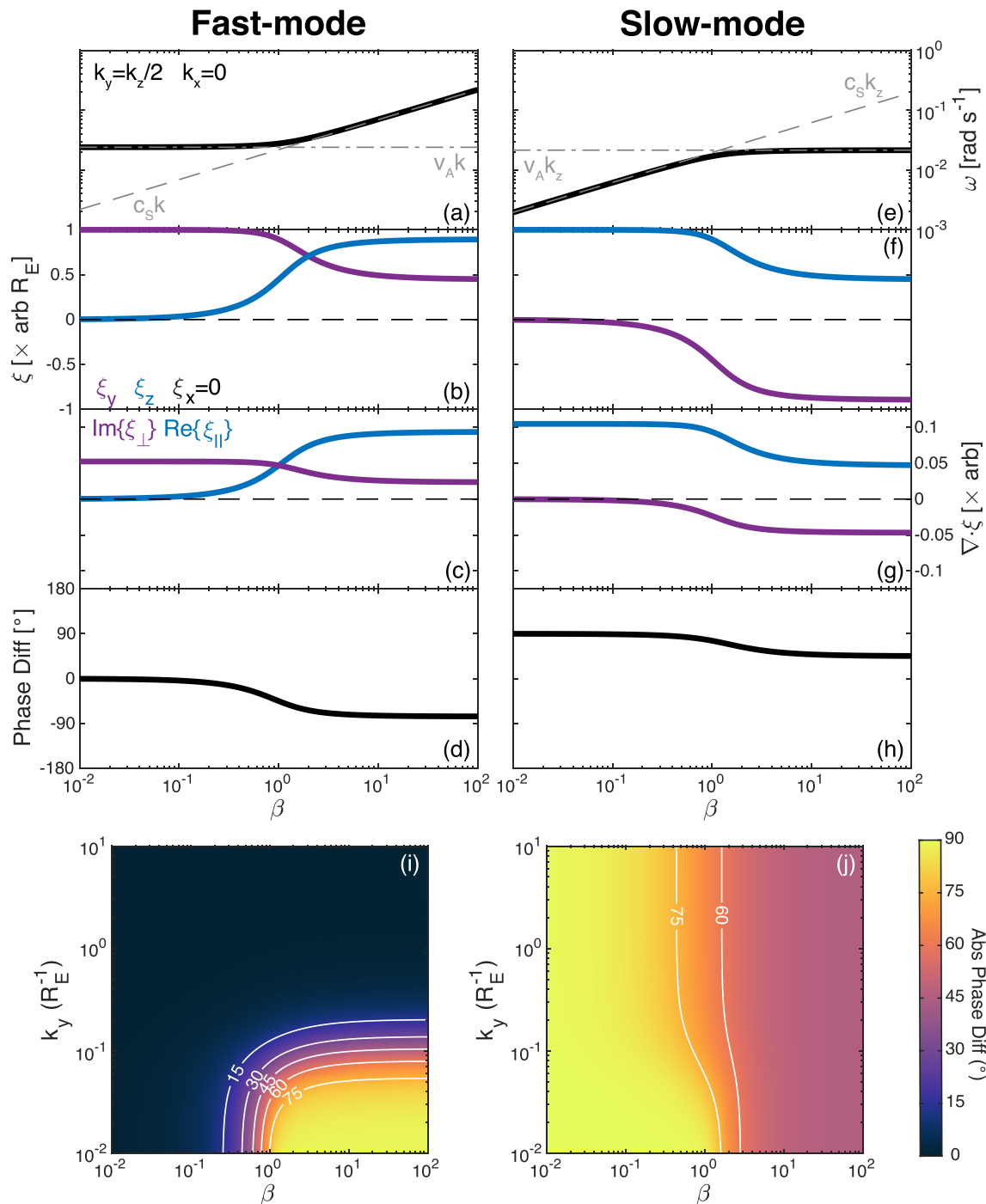


Figure 1. Theoretical results for standing magnetosonic waves. Panels show frequency (a, e), coefficients of displacement (b, f), compression (c, g), and plasma-magnetic field cross-phase (d, h) for the fast (a–d) and slow (e–h) modes as a function of plasma beta. Variations in cross-phase are also shown with both beta and perpendicular wavenumber (i, j).

perpendicular directions (panel c), unlike the propagating case. While for small β perpendicular compression dominates leading to in-phase plasma and magnetic field, under large β parallel compression is largest resulting in $\sim 90^\circ$ cross-phases (panel d) hence zero correlation. Figure 1i shows standing fast-modes differ from in-phase only for $\beta \gtrsim 1$ and $k_y \ll k_z$, due to their high- β asymptotic frequencies $\omega_F \sim c_s k$ (panel a).

Figures 1e–1h similarly shows standing slow-modes. Here displacement coefficients have opposite signs and vary from predominantly parallel to perpendicular with increasing β . For small β , this results in parallel compression

dominating (panel g) and thus quadrature between plasma and magnetic field (panel h), like for high- β standing fast-modes. At large β though, perpendicular and parallel compressions are of similar magnitudes yielding $\sim 45^\circ$ cross-phases or 50% correlation of variance (rather than anticorrelation). Panel j shows results are insensitive to k_y , due to the slow-mode's asymptotic frequencies depending only on k_z (panel e). Thus slow-modes with parallel standing structure do not exhibit the usual plasma–magnetic field anti-phase.

It is worth stressing both modes are constructed from a superposition of waves which individually do satisfy the usual plasma–magnetic field correlations. It is their interference, particularly along the field, that results in anomalous cross-phases.

2.1.2. Surface Waves

The reflective ionosphere also leads to surface eigenmodes on boundaries such as the magnetopause and plasma-pause (Archer et al., 2019; Chen & Hasegawa, 1974; He et al., 2020; Plaschke & Glassmeier, 2011). To investigate plasma–magnetic field relations for magnetopause surface eigenmodes (MSE) we must numerically solve the linearized MHD equations for compressible plasmas given by (see Text S1 in Supporting Information S1)

$$\begin{pmatrix} k_x^2(v_A^2 + c_S^2) + k_z^2v_A^2 - \omega^2 & k_xk_y(v_A^2 + c_S^2) & -ik_xk_zc_S^2 \\ k_xk_y(v_A^2 + c_S^2) & k_y^2(v_A^2 + c_S^2) + k_z^2v_A^2 - \omega^2 & -ik_yk_zc_S^2 \\ ik_xk_zc_S^2 & ik_yk_zc_S^2 & c_S^2k_z^2 - \omega^2 \end{pmatrix} \begin{pmatrix} \xi_x \\ \xi_y \\ \xi_z \end{pmatrix} = 0 \quad (14)$$

We apply the frequency from incompressible theory (Equation 9), which Pu and Kivelson (1983b) showed is similar to the quasi-fast numerical solution. We do not require precise eigenfrequencies, depending on conditions from both half-spaces, as we are only concerned with perturbations in the magnetosphere. The normal wavenumber k_x is set by the magnetosonic relation (Equation 10), which has a singularity at critical plasma β .

$$\beta_{\text{crit}} = \frac{2}{\gamma \left[\left(\frac{k_z v_A}{\omega_{\text{Su}}} \right)^2 - 1 \right]} \quad (15)$$

$$\approx \frac{2}{\gamma \left[\left(\frac{n_{\text{msh}}}{n_{\text{sph}}} \right)^2 - 1 \right]} \quad (16)$$

For typical dayside outer magnetosphere conditions this is small but finite at ~ 0.1 . Around β_{crit} under some conditions $k_x^2 > 0$, corresponding to body modes which are neglected here. Using Pu and Kivelson (1983a), we confirmed the propagating surface waves are quasi-fast with correlated magnetospheric plasma and magnetic field. Standing wave solutions were then found through the null space of Equation 14's matrix by singular value decomposition. Only one independent solution existed for the range of conditions considered.

Figure 2 shows the variation of standing surface waves with β for $k_y = 0$. We find transitions across β_{crit} in normal wavenumber (panel a), displacement coefficients (panel b), and compressions (panel c). Below β_{crit} normal (purple) and field-aligned (blue) displacement coefficients have opposite signs but their compressions have the same sense, hence standing quasi-fast surface modes retain correlated plasma (black line in panel c) and magnetic field (purple). Note for $\beta \rightarrow 0$ only perpendicular displacements exist as there is no pressure to couple motion along the field, whereas as $\beta \rightarrow \beta_{\text{crit}}$ displacements tend toward predominantly field-aligned. Above β_{crit} we find the two displacement coefficients have the same signs, the field-aligned component having reversed across the transition. Displacements are field-aligned near β_{crit} , but as β increases the two components become equal in magnitude. Compressions perpendicular and parallel to the field are oppositely-signed. Given the greater magnitude of parallel motion for $\beta > \beta_{\text{crit}}$, the result is anticorrelated plasma and magnetic field. In the limit $\beta \rightarrow \infty$ parallel and perpendicular compressions cancel, corresponding to incompressibility as expected.

Figures 2d–2i shows results across azimuthal wavenumbers and plasma β 's. The change of sign in parallel displacement (panel f) across β_{crit} with no such change in the perpendicular components (panels d–e) remains for all k_y . This again results in reversal in parallel compression (panel h) but not perpendicular (panel g). Hence the plasma (panel i) becomes anticorrelated to the magnetic field (panel g) above β_{crit} despite the standing surface modes being quasi-fast. Note that as k_y increases, waves become less compressional in all directions.

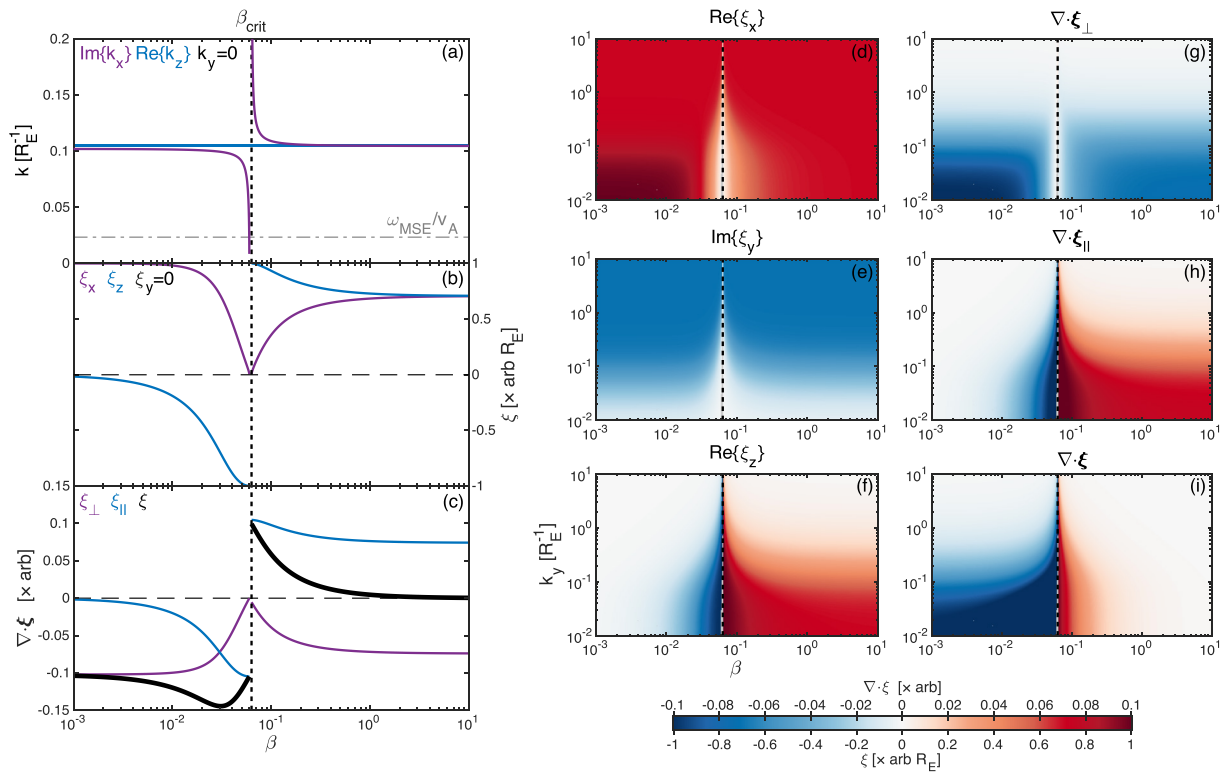


Figure 2. Theoretical results for standing surface waves. Panels show wavenumber (a), coefficients of displacement (b), and compression (c) as a function of plasma beta. Variations in displacement (d–f) and compression (g–i) are also shown with both beta and azimuthal wavenumber.

These standing wave solutions can again be thought of as a superposition of two quasi-fast surface modes propagating oppositely along the field (cf. Plaschke & Glassmeier, 2011). Anomalous anticorrelation above β_{crit} is a result of the wave interference, as was the case for standing body modes also.

2.2. Inhomogeneous Plasma

Inhomogeneity in the background might also affect plasma–magnetic field relations. We introduce a range of small linear density gradients in x to our box model, shown as colors in Figure 3a. These alter the Alfvén speed profiles (panel b). A cold ($\beta = 0$) plasma is used to eliminate slow-modes and the anomalous effects from Section 2.1. We consider magnetopause surface waves, with frequency again from Equation 9, since these have the largest normal scales of magnetospheric MHD eigenmodes (Archer et al., 2022). The WKB (Wentzel–Kramers–Brillouin) solution for magnetospheric displacement are (see Text S2 in Supporting Information S1).

$$\xi_x(x) = \frac{1}{\sqrt{\kappa(x)}} \exp \left\{ i \int_0^x \kappa(s) ds \right\} \exp \left\{ \frac{1}{2} \int_0^x \zeta(s) ds \right\} \quad (17)$$

$$\xi_y(x) = -\frac{ik_y}{k_x^2(x)} \xi_x'(x) \quad (18)$$

$$\xi_z = 0 \quad (19)$$

where primes indicate differentiation in x and

$$\kappa^2(x) = k_x^2(x) + \frac{1}{2} \zeta'(x) - \frac{1}{4} \zeta^2(x) \quad (20)$$

$$\zeta(x) = \frac{k_y^2}{k_x^2(x) [k_x^2(x) + k_y^2]} \frac{\omega^2}{v_A^2(x)} \frac{\rho_0'}{\rho_0(x)} \quad (21)$$

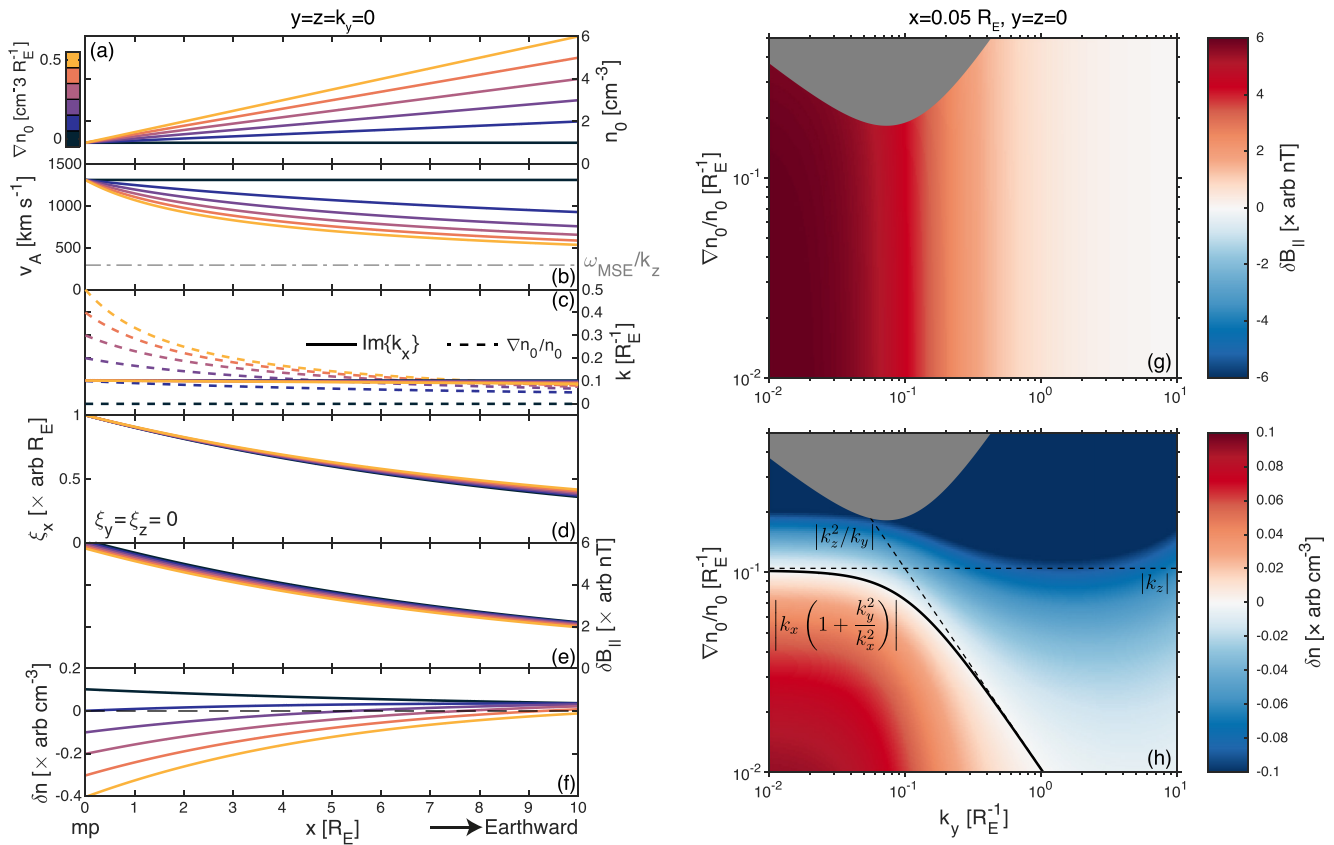


Figure 3. Theoretical results for inhomogeneous density. Panels show, for a range of density gradients, the background density (a), Alfvén speed (b), normal wavenumber and proportional density gradient (c), normal displacement, and magnetic field (e) and density (f) perturbations with distance. Also shown are magnetic field (g) and density (h) perturbations as functions of azimuthal wavenumber and density gradient. Gray areas depict >5% errors in the WKB approximation.

$$k_x^2(x) = -k_y^2 - k_z^2 + \frac{\omega^2}{v_A^2(x)} \quad (22)$$

Figures 3c and 3d show for $k_y = 0$ the normal wavenumber and thus displacement are insensitive to these density gradients. Magnetic field fluctuations (Equation 3; panel e) are due to perpendicular compression only as a uniform field is used, thus vary similarly to ξ_x . On the other hand, density oscillations (Equation 1) include effects of both the wave's inherent perpendicular compression as well as perpendicular advection of plasma with a different background density. There are no pressure perturbations as $\beta = 0$. The density compression has the same sign as the magnetic field. However, due to the sense of the gradient and wave pattern, advection opposes compression. As the density gradient increases the sign of the density perturbations reverses, as demonstrated in panel f. Using Equation 1, this occurs when

$$\begin{aligned} |\xi \cdot \nabla n_0| &> n_0 |\nabla \cdot \xi| \\ \left| \frac{n'_0}{n_0} \xi_x \right| &> |\xi'_x + ik_y \xi_y| \\ &> \left| \left(1 + \frac{k_y^2}{k_x^2} \right) \xi'_x \right| \\ \left| \frac{n'_0}{n_0} \right| &> \left| k_x \left(1 + \frac{k_y^2}{k_x^2} \right) \right| \end{aligned} \quad (23)$$

in other words, when the scale of the density gradient is shorter than that of the wave. Indeed reversals occur approximately (to within WKB's accuracy) when the two scales cross in panel c. Figure 3h shows density

fluctuations near the magnetopause for a range of both density gradients and azimuthal wavenumbers. Equation 23 is given by the black line, which clearly separates positive and negative. The magnetic field in this parameter space (panel g), however, remains positive throughout, though decreasing in amplitude with k_y . Therefore fast-modes, in this case surface waves, can have anticorrelated density and magnetic field due to inhomogeneity in the background plasma.

3. Simulation

We now investigate if similar effects occur within a more representative magnetosphere through global MHD simulations. We use a published high-resolution Space Weather Modeling Framework (SWMF; Tóth et al., 2005, 2012) run simulating the magnetospheric response to a 1 min solar wind density pulse (see Table S1 in Supporting Information S1 for setup; Hartinger et al., 2015; Archer et al., 2021, 2022, 2023). Previous studies have demonstrated a large-amplitude transient response occurs followed by global damped 1.8 mHz compressional waves, the latter corresponding to MSE: surface waves with parallel standing structure. MSE stands against the magnetosheath flow across the dayside, also seeding tailward propagating boundary disturbances to the flanks. Amplitudes decay with distance from the magnetopause and phase motion ($\ll v_A$) toward the boundary occurs, in line with damped compressible surface waves. Coupling to body eigenmodes occurs on the nightside where eigenfrequencies match. Density and pressure oscillations in this run have yet to be studied.

We extract equilibrium conditions through 30 min median filtering of each quantity, subsequently smoothed using 10 min moving averages. Figures S1a–S1c in Supporting Information S1 shows the equatorial density, pressure, and magnetic field equilibria. The magnetospheric plasma β varies substantially (Figure S1d in Supporting Information S1): ~ 0.1 – 0.4 in the dayside outer magnetosphere ($r \gtrsim 7 R_E$); ~ 2 – 25 in both outer flanks ($|y| \gtrsim 10 R_E$); and up to ~ 150 in the magnetotail plasma sheet. We compute 3-dimensional gradients of these backgrounds using second order 5-point finite differencing (see Figures S1e–S1g in Supporting Information S1 for proportional magnitudes). Perturbations about equilibrium are shown in Movie S1 across the equatorial plane and maps of their Median Absolute Deviations (MAD), used as a robust measure of variability and thus amplitude, are given in Figures S1h–S1j in Supporting Information S1.

Movie S1 clearly shows the density pulse's initial transient response consists of dayside compression of the geomagnetic field, density, and pressure. Once the launched compressional wave front reflects off the simulation inner boundary at $t = 7$ min (Archer et al., 2021), plasma becomes rarefield while the magnetic field is still enhanced, indicating these are no longer in-phase. Following this ($t \gtrsim 10$ min) MSE is established on the dayside, as sufficient time has passed for poleward propagating surface waves to reflect off the simulation inner boundary. Plasma and magnetic field perturbations have opposite signs during MSE. Similar results occur in the flanks, though at later times owing to propagation of the pulse and launched waves.

From the analytic signals of plasma and magnetic field oscillations (computed via Hilbert transforms in time) we calculate instantaneous cross-phases, also shown in Movie S1. These confirm the plasma and magnetic field are mostly in-phase (green) initially but change to predominantly anti-phase (blue). Figure 4 shows cross-phase time-series from representative locations in the outer dayside (square, panel r) and flank (circle, panel n). They are almost the same for density and pressure. In the flanks the cross-phase settles to $160 \pm 20^\circ$ (mean and spread), close but not exactly anti-phase. This is also apparent in the time-series (black lines in panels k–m). On the dayside we find somewhat similar results at $150 \pm 30^\circ$, with the offset again clear in the time-series (panels o–r). Rippling in cross-phase occurs as amplitudes decreases, likely artifacts of the Hilbert transform (e.g., Hong et al., 2021).

Anticorrelation of plasma and magnetic field is also clear in Spearman's rank correlation coefficients (Figures 4a and 4b). This statistic is more representative of the monotonic relationship throughout the interval, not biasing toward the larger-amplitude transient like Pearson's. Both panels indicate significant anticorrelation ($-0.75 \lesssim r_s \lesssim -0.5$) between magnetic field and plasma throughout the outer magnetosphere. Note that tailward of the terminator a region of strong correlation emerges around the open–closed field line boundary (black and white dashed line), a proxy for the magnetopause. These correspond to the amplitude of boundary oscillations evident in the movie, thus are oscillatory transitions between magnetospheric and magnetosheath plasma. The waves in this simulation are fast-modes, given agreement in theoretical eigenfrequency (Hartinger et al., 2015) and large perpendicular Poynting fluxes (Archer et al., 2021), yet exhibit anticorrelated plasma and magnetic fields.

To understand this we estimate the linear contributions to the perturbations due to compression and advection (Equations 1–3). Since the simulation does not output displacement we instead use the extracted velocity fluctuations in

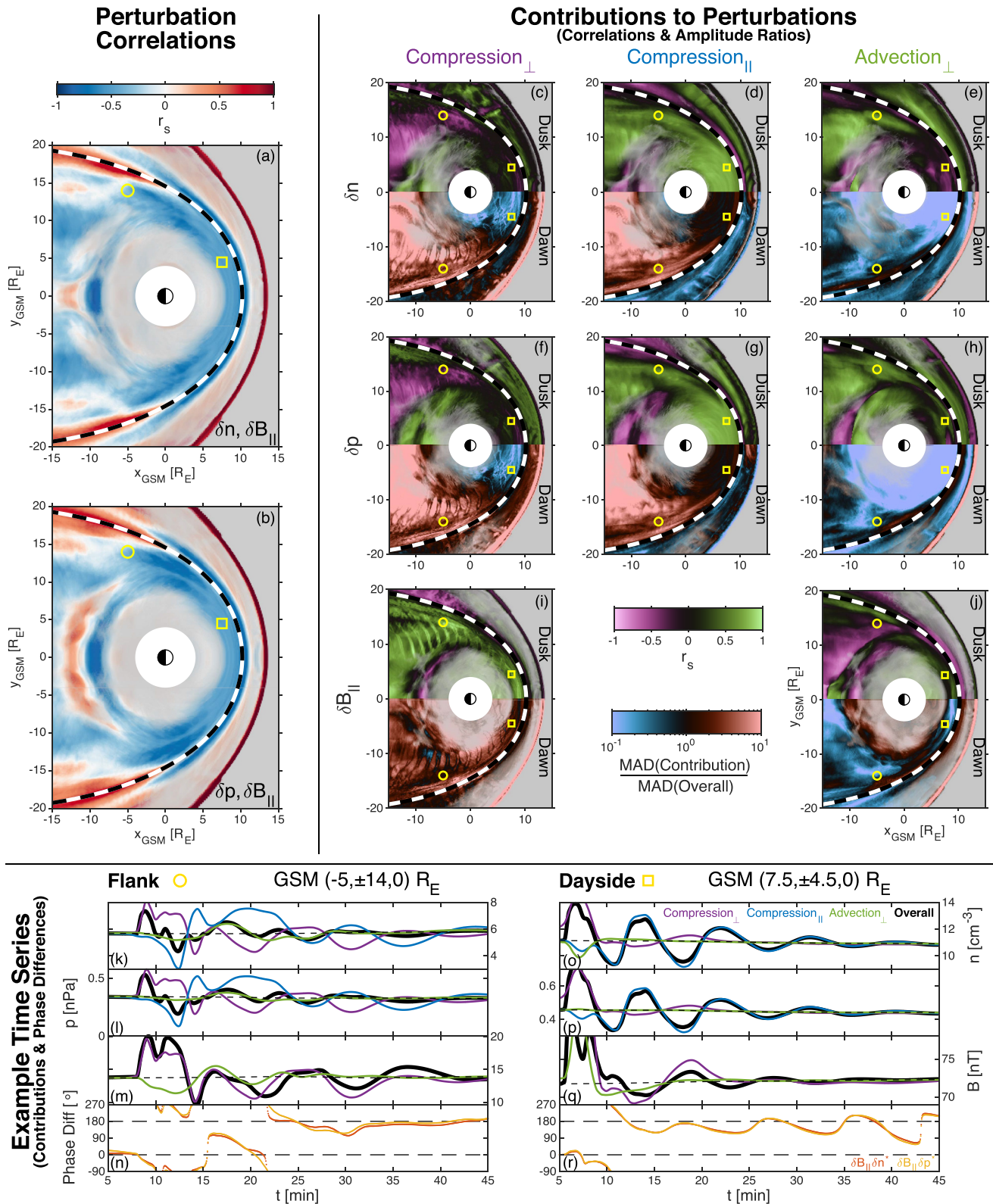


Figure 4. Global MHD simulation results in the equatorial plane. (a–b) Correlation coefficients between the magnetic field and density (a) or pressure (b) perturbations. Grays indicate low-amplitudes. (c–j) Linear contributions to density (c–e), pressure (f–h), and magnetic field (i–j) perturbations due to the effects of perpendicular (c, f, i) and parallel (d, g) compression, and perpendicular advection (e, h, j). Shown are correlation coefficients (top half) and amplitude ratios (bottom half) between the contributions and overall results. (k–r) Example time-series in the flank (k–n) and dayside (o–r) comparing the contributions to the overall fluctuations for each quantity, and magnetic field–plasma cross-phases.

these equations at each time, yielding the perturbations' time-derivatives. While these are sufficient to arrive at our conclusions which we checked (Figure S2 in Supporting Information S1), rates-of-change are less intuitive than the perturbations themselves hence we integrate them in time. As this could result in accumulation of numerical errors, we try to limit these. Smooth piecewise-polynomials of the rates-of-change using Akima's (1970) algorithm are constructed and analytically integrated. This is performed backwards in time to reduce errors associated with the transient, which is large-amplitude and poorly resolved by the 30 s simulation output cadence. Finally, accumulated non-oscillatory trends are removed by applying the same median filter as before. Results in the equatorial plane are shown in Movie S2 for the afternoon sector only, since the simulation is dawn–dusk symmetric. This plane is a field-aligned velocity node (Archer et al., 2022) thus we neglect displaying parallel advection. It is clear, despite the careful processing, artifacts still remain at the start of the interval, such as large initial values and banding patterns of similar scale to the transient. Nonetheless, following the transient ($t \gtrsim 15$ –20 min) results appear reliable. Figures 4c–4j compare the linear contributions to the simulation output. In each panel the top half (dusk sector) shows Spearman correlations and the bottom (dawn) shows ratios of MAD (remember we have dawn–dusk symmetry). Where banding artifacts remain in this analysis, values intermediate between the peaks/troughs should be considered (cf. Figure S2 in Supporting Information S1). Time series of these contributions (colors) from locations on the dayside (panels o–r) and flank (panels k–n) are also shown and compared to the simulation output (black).

We first look at contributions to the magnetic field. Movie S2 shows throughout the run perpendicular compression of plasma is much larger than advection of magnetic field inhomogeneities. Figure 4j indicates advection is poorly (and often anti-) correlated to the overall perturbations. Exceptions to this occur close to the magnetopause, though their amplitudes are about an order of magnitude too small. This is also clear in example time-series on the dayside (panel q) and flank (panel m), where advection (green) poorly follows the overall result (black). In contrast, perpendicular compression (panel i) shows good correlation. The amplitude of this term is also similar to the simulation output. Finally, the two example time-series (panels m, q) show perpendicular compression (purple) reasonably tracks the actual field compressions (with slight offsets likely due to the processing). Note the double-peaked structure of the transient is not well captured as plasma displacements are large with the boundary itself moving, violating the linear assumptions used. Therefore, we find the magnetic field oscillations are largely dictated by perpendicular compression.

Looking at the linear contributions to the plasma in Movie S2, density and pressure exhibit similar patterns. On the dayside, the pulse's arrival causes strong perpendicular compression with the other two terms being small and of opposite sign (see also Figures 4o–4p). However, once MSE is established parallel compression dominates, due to the larger-amplitude of standing structures in the parallel velocity compared to perpendicular (Archer et al., 2022). Only parallel compression shows strong correlation and similar amplitudes to the resultant plasma perturbations here (Figures 4c–4h). Indeed, the simulation output follows parallel compression (blue) very well on the dayside (panels o–p). Thus despite low dayside plasma β , the finite pressure coupling perpendicular and parallel fluid motion has a strong influence on the waves. β is found to be ~ 3 –10X the critical value (Equation 15). Therefore, anticorrelation of plasma and magnetic field arises from the interference pattern along the field of oppositely propagating surface waves. In the flanks, Movie S2 reveals both parallel and perpendicular compression are strong but with opposite signs, with perpendicular compression being anticorrelated with the overall perturbations (Figures 4c–4h). Both compressional terms overestimate the resultant amplitude. This is because the flanks have high β , corresponding to near-incompressibility, which is also apparent in the time-series (panels k–l). Despite perpendicular advection being the weakest term, it correlates well and has generally similar amplitude to the simulation output. As this term (green) is of opposite sign to the perpendicular compression (purple), the result is an overall anticorrelation between plasma and magnetic field. Therefore, in the flanks the advection of plasma non-uniformities becomes important since the wave is near-incompressible.

Overall, the simulation demonstrates that fast-mode waves can have anticorrelated plasma and magnetic field. We see evidence of both theoretical effects described in Section 2 at different locations within the magnetosphere, due to the conditions present.

4. Discussion

We have shown through both theory and a global MHD simulation that magnetosonic body and surface waves can have altered magnetic field–plasma (density/pressure) correlations when the wave has standing structure along the magnetic field or if the plasma is inhomogeneous. For standing body waves anomalous cross-phases may

occur of: $\sim 90^\circ$ for fast-modes at high- β and small perpendicular wavenumber, or for slow-modes at low- β ; and $\sim 45^\circ$ for slow-modes at high- β . Therefore, standing slow-modes do not show the usual anticorrelation between plasma and magnetic field. Quasi-fast surface eigenmodes, however, may exhibit anticorrelated plasma and magnetic field, which occurs above a critical plasma β . These standing wave effects are a result of the interference pattern between counter-propagating waves along the field. Additionally, if the background environment is inhomogeneous, a magnetosonic wave advects plasma with a different background, which can overcome the sense of the wave's inherent compression. This becomes important if the scale of the gradient is shorter than the wave's scale, or if the wave is near-incompressible. Across geospace both of these MHD wave effects are likely most important within the magnetosphere since ULF waves are reflected by the ionosphere and their wavelengths are of the order of the system size, however we do not preclude they could also occur elsewhere.

This study focused only on Ideal-MHD, where the isotropic pressure strongly couples motion perpendicular and parallel to the field. However, space plasmas are collisionless and anisotropic, which can be incorporated into MHD through double-adiabatic laws specified by two exponents. Studies exploring propagating waves in these theories have shown density and magnetic field can be correlated for slow-modes whereas the usual relation persists for fast-modes (Hau & Sonnerup, 1983; Hau & Wang, 2007). It is likely the effects presented here would still be present, though we leave exploring the parameter spaces to future work. Highly anisotropic plasmas can also be unstable to (drift-) mirror modes (e.g., Génot et al., 2001; Hasegawa, 1969), also characterized by anti-correlated magnetic field and density. Statistical studies of the outer magnetosphere often attribute observed anti-correlations to this mode, despite the instability criterion not always being satisfied (Nishi et al., 2018; Vaivads et al., 2001; Zhu & Kivelson, 1991, 1994). Magnetopause surface waves might account for some of these observations. Several additional tests for identifying kinetic wave modes exist (Schwartz et al., 1996) such as compressibility (Denton et al., 1995), particle distributions (Leckband et al., 1995), or plasma frame frequency.

The effects presented here might be accounted for in multi-spacecraft missions (such as MMS or the upcoming HelioSwarm) as, when suitably separated, they are able to track phase motion and measure gradients, hence can compute directly the contributions of compression and advection to observed waves. However, with less than four local observation points that is not generally possible. Nonetheless, standing structure along the field could be inferred through reactive field-aligned Poynting flux (Archer et al., 2022; Kokubun et al., 1977) and magnitudes of plasma gradients might be ascertained through background trends as spacecraft orbit. We, therefore, recommend wave observations relying on the plasma–magnetic field correlation employ these additional checks to be confident on their fast-, slow-, or mirror-mode nature.

Data Availability Statement

Simulation results have been provided by the Community Coordinated Modeling Center (CCMC) at Goddard Space Flight Center using the SWMF and BATS-R-US tools developed at the University of Michigan's Center for Space Environment Modeling (CSEM). This data is available at https://ccmc.gsfc.nasa.gov/results/viewrun.php?domain=GM&runnumber=Michael_Hartinger_061418_1.

References

- Akima, H. (1970). A new method of interpolation and smooth curve fitting based on local procedures. *JACM*, 17(4), 589–602. <https://doi.org/10.1145/321607.321609>
- Allan, W. (1982). Phase variation of ULF pulsations along the geomagnetic field-line. *Planetary and Space Science*, 30(4), 339–346. [https://doi.org/10.1016/0032-0633\(82\)90039-3](https://doi.org/10.1016/0032-0633(82)90039-3)
- Archer, M. O., Hartinger, M. D., Plaschke, F., Southwood, D. J., & Rastaetter, L. (2021). Magnetopause ripples going against the flow form azimuthally stationary surface waves. *Nature Communications*, 12(1), 5697. <https://doi.org/10.1038/s41467-021-25923-7>
- Archer, M. O., Hartinger, M. D., Rastaetter, L., Southwood, D. J., Heyns, M., Eggington, J. W. B., et al. (2023). Auroral, ionospheric and ground magnetic signatures of magnetopause surface modes. *Journal of Geophysical Research: Space Physics*, 128(3), e2022JA031081. <https://doi.org/10.1029/2022JA031081>
- Archer, M. O., Hietala, H., Hartinger, M. D., Plaschke, F., & Angelopoulos, V. (2019). Direct observations of a surface eigenmode of the dayside magnetopause. *Nature Communications*, 10(1), 615. <https://doi.org/10.1038/s41467-018-08134-5>
- Archer, M. O., & Plaschke, F. (2015). What frequencies of standing surface waves can the subsolar magnetopause support? *Journal of Geophysical Research: Space Physics*, 120(5), 3632–3646. <https://doi.org/10.1002/2014JA020545>
- Archer, M. O., Southwood, D. J., Hartinger, M. D., Rastaetter, L., & Wright, A. N. (2022). How a realistic magnetosphere alters the polarizations of surface, fast magnetosonic, and alfvén waves. *Journal of Geophysical Research: Space Physics*, 127(2), e2021JA030032. <https://doi.org/10.1029/2021JA030032>
- Chen, L., & Hasegawa, A. (1974). A theory of long-period magnetic pulsations: 2. Impulse excitation of surface eigenmode. *Journal of Geophysical Research*, 79(7), 1033–1037. <https://doi.org/10.1029/JA079i007p01033>

Acknowledgments

This research was supported by the International Space Science Institute (ISSI) in Bern, through ISSI International Team project #546 “Magnetohydrodynamic Surface Waves at Earth’s Magnetosphere (and Beyond)” led by MOA and KN. MOA holds a UKRI (STFC/EPSRC) Stephen Hawking Fellowship EP/T01735X/1. DJS was supported by STFC Grant ST/W001071/1. MDH was supported by NASA Grants 80NSSC21K1683 and 80NSSC21K1677. KN was supported by NASA Grant 80NSSC22K0304. For the purpose of open access, the author has applied a Creative Commons Attribution (CC BY) license to any Author Accepted Manuscript version arising.

- Degeling, A. W., Rankin, R., Kabin, K., Rae, I. J., & Fenrich, F. R. (2010). Modeling ULF waves in a compressed dipole magnetic field. *Journal of Geophysical Research*, *115*(A10), A10212. <https://doi.org/10.1029/2010JA015410>
- Denton, R. E., Gary, S. P., Li, X., Anderson, B. J., LaBelle, J. W., & Lessard, M. (1995). Low-frequency fluctuations in the magnetosheath near the magnetopause. *Journal of Geophysical Research*, *100*(A4), 5665–5679. <https://doi.org/10.1029/94JA03024>
- Du, J., Zhang, T. L., Nakamura, R., Wang, C., Baumjohann, W., Du, A. M., et al. (2011). Mode conversion between Alfvén and slow waves observed in the magnetotail by THEMIS. *Geophysical Research Letters*, *38*(7), L07101. <https://doi.org/10.1029/2011GL046989>
- Eastwood, J. P., Balogh, A., Dunlop, M. W., Horbury, T. S., & Dandouras, I. (2002). Cluster observations of fast magnetosonic waves in the terrestrial foreshock. *Geophysical Research Letters*, *29*(22), 2046. <https://doi.org/10.1029/2002GL015582>
- Génot, V., Schwartz, S. J., Mazelle, C., Balikhin, M., Dunlop, M., & Bauer, T. M. (2001). Kinetic study of the mirror mode. *Journal of Geophysical Research*, *106*(A10), 21611–21622. <https://doi.org/10.1029/2000JA000457>
- Hartering, M. D., Angelopoulos, V., Moldwin, M. B., Takahashi, K., & Clausen, L. B. N. (2013). Statistical study of global modes outside the plasmasphere. *Journal of Geophysical Research: Space Physics*, *118*(2), 804–822. <https://doi.org/10.1002/jgra.50140>
- Hartering, M. D., Plaschke, F., Archer, M. O., Welling, D. T., Moldwin, M. B., & Ridley, A. (2015). The global structure and time evolution of dayside magnetopause surface eigenmodes. *Geophysical Research Letters*, *42*(8), 2594–2602. <https://doi.org/10.1002/2015GL063623>
- Hartering, M. D., Takahashi, K., Drozdov, A. Y., X. S., Usanova, M. E., & Kress, B. (2022). ULF wave modeling, effects, and applications: Accomplishments, recent advances, and future. *Frontiers in Astronomy and Space Sciences*, *9*, 867394. <https://doi.org/10.3389/fspas.2022.867394>
- Hasegawa, A. (1969). Drift mirror instability in the magnetosphere. *Physics of Fluids*, *12*, 2642–2650. <https://doi.org/10.1063/1.1692407>
- Hau, L.-N., & Sonnerup, B. U. O. (1983). On slow-mode waves in an anisotropic plasma. *Journal of Geophysical Research*, *88*(17), 853–861. <https://doi.org/10.1029/93GL01706>
- Hau, L.-N., & Wang, B.-J. (2007). On MHD waves, fire-hose and mirror instabilities in anisotropic plasmas. *Nonlinear Processes in Geophysics*, *14*(5), 557–568. <https://doi.org/10.5194/npg-14-557-2007>
- He, F., Guo, R.-L., Dunn, W. R., Yao, Z.-H., Zhang, H.-S., Hao, Y.-X., et al. (2020). Plasmapause surface wave oscillates the magnetosphere and diffuse aurora. *Nature Communications*, *11*(1), 1668. <https://doi.org/10.1038/s41467-020-15506-3>
- Hong, R., Corrodi, S., Charity, S., Baebler, S., Bono, J., Chupp, T., et al. (2021). Systematic and statistical uncertainties of the Hilbert-transform based high-precision FID frequency extraction method. *Journal of Magnetic Resonance*, *329*, 107020. <https://doi.org/10.1016/j.jmr.2021.107020>
- Jacobs, J., Kato, Y., Matsushita, S., & Troitskaya, V. (1964). Classification of geomagnetic micropulsations. *Journal of Geophysical Research*, *69*(1), 180–181. <https://doi.org/10.1029/JZ069i001p00180>
- Kivelson, M. G., Etcheto, J., & Troignon, J. G. (1984). Global compressional oscillations of the terrestrial magnetosphere: The evidence and a model. *Journal of Geophysical Research*, *89*(A11), 9851–9856. <https://doi.org/10.1029/JA089iA11p09851>
- Kivelson, M. G., & Southwood, D. J. (1985). Resonant ULF waves: A new interpretation. *Geophysical Research Letters*, *12*(1), 49–52. <https://doi.org/10.1029/GL012i001p00049>
- Kivelson, M. G., & Southwood, D. J. (1988). Hydromagnetic waves and the ionosphere. *Geophysical Research Letters*, *15*(11), 1271–1274. <https://doi.org/10.1029/GL015i011p01271>
- Kokubun, S., Kivelson, M. G., McPherron, R. L., Russell, C. T., & West, H. I. (1977).OGO 5 observations of Pc5 waves: Particle flux modulations. *Journal of Geophysical Research*, *82*(19), 2774–2786. <https://doi.org/10.1029/JA082i019p02774>
- Leckband, J. A., Burgess, D., Pantellini, F. G. E., & Schwartz, S. J. (1995). Since 2023since 2022since 2019custom range...sort by relevancesort by dateany typereview articles[pdf] academia.eduion distributions associated with mirror waves in the earth's magnetosheath. *Advances in Space Research*, *15*(8–9), 345–348. [https://doi.org/10.1016/0273-1177\(94\)00115-H](https://doi.org/10.1016/0273-1177(94)00115-H)
- Moore, T. E., Gallagher, D. L., Horwitz, J. L., & Comfort, R. H. (1987). MHD wave breaking in the outer plasmasphere. *Geophysical Research Letters*, *14*(10), 1007–1010. <https://doi.org/10.1029/GL014i010p01007>
- Nishi, K., Shiokawa, K., Glassmeier, K.-H., & Mieth, J. Z. D. (2018). Statistical study of phase relationship between magnetic and plasma pressures in the near-Earth nightside magnetosphere using the THEMIS-E satellite. *Journal of Geophysical Research: Space Physics*, *123*(11), 9517–9531. <https://doi.org/10.1029/2018JA025846>
- Plaschke, F., & Glassmeier, K. H. (2011). Properties of standing Kruskal-Schwarzschild-modes at the magnetopause. *Annales Geophysicae*, *29*(10), 1793–1807. <https://doi.org/10.5194/angeo-29-1793-2011>
- Pu, Z.-Y., & Kivelson, M. G. (1983a). Kelvin-Helmholtz instability at the magnetopause: Energy flux into the magnetosphere. *Journal of Geophysical Research*, *88*(A2), 853–861. <https://doi.org/10.1029/JA088iA02p00853>
- Pu, Z.-Y., & Kivelson, M. G. (1983b). Kelvin-Helmholtz instability at the magnetopause: Solution for compressible plasmas. *Journal of Geophysical Research*, *88*(A2), 841–852. <https://doi.org/10.1029/JA088iA02p00841>
- Radoski, H. R. (1971). A note on the problem of hydromagnetic resonances in the magnetosphere. *Planetary and Space Science*, *19*(8), 1012–1013. [https://doi.org/10.1016/0032-0633\(71\)90152-8](https://doi.org/10.1016/0032-0633(71)90152-8)
- Samson, J. C., Harrold, B. G., Ruohoniemi, J. M., Greenwald, R. A., & Walker, A. D. M. (1992). Field line resonances associated with MHD waveguides in the magnetosphere. *Geophysical Research Letters*, *19*(5), 441–444. <https://doi.org/10.1029/92GL00116>
- Schwartz, S. J., Burgess, D., & Moses, J. J. (1996). Low-frequency waves in the Earth's magnetosheath: Present status. *Annales Geophysicae*, *14*(11), 1134–1150. <https://doi.org/10.1007/s00585-996-1134-z>
- Southwood, D. J. (1968). The hydromagnetic stability of the magnetospheric boundary. *Planetary and Space Science*, *16*(5), 587–605. [https://doi.org/10.1016/0032-0633\(68\)90100-1](https://doi.org/10.1016/0032-0633(68)90100-1)
- Southwood, D. J. (1974). Some features of field line resonances in the magnetosphere. *Planetary and Space Science*, *22*(3), 483–491. [https://doi.org/10.1016/0032-0633\(74\)90078-6](https://doi.org/10.1016/0032-0633(74)90078-6)
- Tóth, G., Sokolov, I. V., Gombosi, T. I., Chesney, D. R., Clauer, C. R., De Zeeuw, D. L., et al. (2005). Space weather modeling framework: A new tool for the space science community. *Journal of Geophysical Research*, *110*(A12), A12226. <https://doi.org/10.1029/2005JA011126>
- Tóth, G., van der Holst, B., Sokolov, I. V., De Zeeuw, D. L., Gombosi, T. I., Fang, F., et al. (2012). Adaptive numerical algorithms in space weather modeling. *Journal of Computational Physics*, *231*(3), 870–903. <https://doi.org/10.1016/j.jcp.2011.02.006>
- Turc, L., Roberts, O. W., Verscharen, D., Dimmock, A. P., Kajdič, P., Palmroth, M., et al. (2022). Transmission of foreshock waves through Earth's bow shock. *Nature Physics*, *19*(1), 78–86. <https://doi.org/10.1038/s41567-022-01837-z>
- Vaivads, A., Baumjohann, W., Haerendel, G., Nakamura, R., Kucharek, H., Klecker, B., et al. (2001). Compressional Pc5 type pulsations in the morningside plasma sheet. *Annales Geophysicae*, *19*(3), 311–320. <https://doi.org/10.5194/angeo-19-311-2001>
- Yao, S., He, J.-S., Tu, C.-Y., Wang, L.-H., & Marsch, E. (2013). Small-scale pressure-balanced structures driven by oblique slow mode waves measured in the solar wind. *The Astrophysical Journal*, *774*(1), 59. <https://doi.org/10.1088/0004-637X/774/1/59>

- Zhang, W., Nishimura, Y., Wang, B., Hwang, K.-J., Hartinger, M. D., Donovan, E. F., et al. (2022). Identifying the structure and propagation of dawnside Pc5 ULF waves using space-ground conjunctions. *Journal of Geophysical Research: Space Physics*, *127*(12), e2022JA030473. <https://doi.org/10.1029/2022JA030473>
- Zhu, X., & Kivelson, M. G. (1991). Compressional ULF waves in the outer magnetosphere: 1. Statistical study. *Journal of Geophysical Research*, *96*(A11), 19451–19467. <https://doi.org/10.1029/91JA01860>
- Zhu, X., & Kivelson, M. G. (1994). Compressional ULF waves in the outer magnetosphere: 2 a case study of Pc5 type wave activity. *Journal of Geophysical Research*, *99*(A1), 241–252. <https://doi.org/10.1029/93JA02106>